Preprints of the 9th International Symposium on Robot Control (SYROCO'09)
The International Federation of Automatic Control
Nagaragawa Convention Center, Gifu, Japan, September 9-12, 2009

A cardiac motion compensation device based on gyroscopic effect

J. Gagne O. Piccin E. Laroche J. Gangloff

LSIIT (UMR CNRS-UdS 7005), Strasbourg University, France,
(e-mails: julien.gagne@lsiit.u-strasbg.fr,
olivier.piccin@insa-strasbourg.fr, laroche@unistra.fr,
jacques.gangloff@unistra.fr)

Abstract: The difficulties encountered in preventing the cardiac motion is a hindrance to the development of recent less invasive techniques in the field of beating heart surgery. Some solutions were developed already in order to solve this problem, inducing specific and cumbersome equipment. The alternative described herein is based on a compact simple device using gyroscopic effect, intended to be adaptable to existing equipment and which is non-grounded. The presented work is a preliminary study of such a system. After exposing the principle and dynamical equations we present the device design process which was carried out and finally discuss the control strategy based on Linear Quadratic Regulator (LQR) synthesis and its simulation results.

Keywords: surgical robotics, beating heart surgery, gyroscopic effect, LQR synthesis

1. INTRODUCTION

Nowadays the development of new surgical techniques is focused on reducing the invasiveness. Thanks to the technology and the use of embedded cameras, laparoscopic surgery has known a great development during the last years and is now widely used in particular for gastrointestinal, gynecological and urological surgery. Extending these techniques to other fields is a crucial challenge since their benefits are numerous: it reduces among other things infectious hazard, scars size, hospital stay and patient recovery time. However, in some cases as for cardiac surgery the use of minimally invasive techniques is not applicable easily as pointed out Mack (2006) even though it could heavily improve surgery quality. Indeed a classical operation as coronary bypass implies heavy invasive steps such as sternum dissection, rib cage opening and extra corporeal circulation which are the main complication causes and could be avoided using minimally invasive beating heart surgery. Nevertheless dealing with the heart motion is the main hindrance to the use of such techniques.

Fig. 1. Example of a cardiac stabilizer acting by pressure from CTS Guidant.

However, some beating heart coronary bypasses were performed by open and laparoscopic ways as did Loisance et al. (2005). In these cases, the cardiac motion problem has been solved by using passive stabilizers illustrated in Fig. 1 which are constituted by a stiff rod maintaining the interesting area of the heart thanks to two fingers by pressure or suction. But with these stabilizers the residual motion due to the device flexibility is not negligible as highlighted Lemma et al. (2005). As an alternative, some solutions based on active compensation as the one by Bachta et al. (2008) were developed, demonstrating the efficiency of such an approach, but implying the use of specific or cumbersome equipment. The purpose of the work presented herein consists in designing a device assuming the function of active stabilization and intended to be connected with existing commercial instruments. The size and wheight are also considered as critical criterions to design a device compatible with the highly constrained surgical environment.

For this purpose, we chose to take advantage of the gyroscopic effect. This mechanical property is known to permit the generation of torques without the need to be linked to the ground. Various applications exploiting this concept can be found in the literature. For instance Townsend et al. (2007) developed stabilization system for ships. Attitude control in zero gravity environments was carried out for satellites by Lappas et al. (2002) and for submarine robots by Thornton et al. (2007). Higashimata et al. (1998) worked on antisismic building stabilization. A non-grounded haptic interface was developed by Yano et al. (2003). This principle is usually exploited for large and heavy structures but we propose to use it at a smaller scale within the framework of cardiac stabilization for beating heart surgery. However, since the system presented here is independent from the surgical instrument, the

concept can be extended to other applications needing structural stabilization in similar frequency domain.

The work presented in this paper is a preliminary study concerning such a system. First we explain the principle and equations then the mechanical design of the device which was carried out and finally the control aspects and simulations.

2. PRINCIPLE AND THEORY

The rigid-body model of the gyroscopic compensation system depicted in Fig. 2 is composed of an inertia wheel ④ rotating at a constant high speed thanks to a first actuator. It constitutes the gyroscope. This wheel is attached to a gimbal ③ which rotation can be controlled with a second actuator. The whole system is attached to the rod of the passive stabilizer ②. The passive stabilizer is connected to the ground by a massless part ① using two revolute joints. Thus, the resulting system is composed of four links serially assembled with four revolute joints.

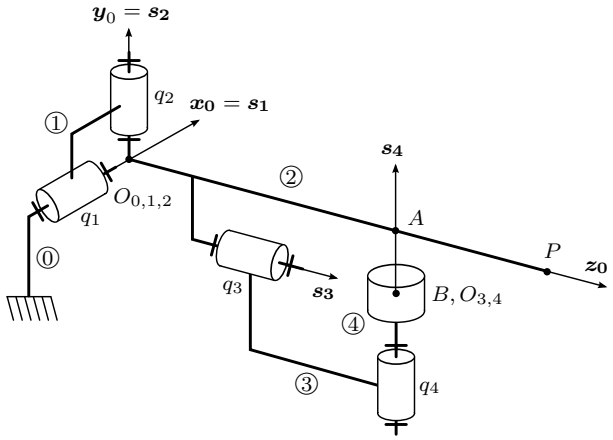

Fig. 2. System description in its reference configuration.

The geometry of the mechanism can be described using the method of successive screw displacements defined by Tsai (1999). $\mathcal{F}_0 = (O_0, \boldsymbol{x_0}, \boldsymbol{y_0}, \boldsymbol{z_0})$ denotes the base frame with respect to which the displacements are measured. The configuration shown in Fig. 2 corresponds to the system reference position. The i-th joint axis of the mechanism is defined by the couple $(\boldsymbol{s_i}, \boldsymbol{s_{O_i}})$ where $\boldsymbol{s_i}$ is the unit vector of the axis and $\boldsymbol{s_{O_i}} = \boldsymbol{O_0 O_i}$ defines the position of a point O_i of the axis. Table 1 and Fig. 2 provide the joint axis definition of the mechanism. The flexibilities of the stabilizer are modeled by two torsional springs and dampers of coefficient k and f mounted on the two first revolute joints.

Table 1. Joint axis definition for the reference configuration of Fig. 2.

	$\boldsymbol{s_i}$ in $\mathcal{F}_0$	$\boldsymbol{s_{O_i}}$ in $\mathcal{F}_0$
i=1	$[1\ 0\ 0]^T$	$[0\ 0\ 0]^T$
i=2	$[0\ 1\ 0]^T$	$[0\ 0\ 0]^T$
i=3	$[0\ 0\ 1]^T$	$[0\ -l_B\ l_A]^T$
i=4	$[0\ 1\ 0]^T$	$[0\ -l_B\ l_A]^T$

The four revolute joints are parameterized with the angles q_i whose sine and cosine are abbreviated as s_i and c_i.

In operating conditions, the angles q_1 and q_2 are supposed to be small and the rotor spins at a constant high speed $\dot{q}_4 = \Omega$. The gimbal mass as well as the gyroscope moments of inertia other than the one with respect to its revolution axis are neglected. The effects of gravity are also assumed to be negligible.

We introduce the following parameters for the system modeling. The total length of the stabilizer is L and its distal-end point is P. J_2 denotes its moment of inertia with respect to the axes $(O_0, \boldsymbol{s_1})$ and $(O_0, \boldsymbol{s_2})$. The mass of the gyroscope is m_4 and its moment of inertia with respect to its revolution axis $(B, \boldsymbol{s_4})$ is B_4. The forces F_x and F_y denote the projections in the base frame $\mathcal{F}_0$ of the cardiac force applied at point P. T_{23} and T_{34} represent respectively the torques applied by the motors on the gimbal and the rotor. The following Lagrange equations were calculated, linearized around the position $(q_1, q_2) = (0, 0)$ and simplified using the previous assumptions.

$$\begin{aligned}\mathcal{L}_{q_1} : &\left[J_2 + m_4\left(l_A^2 + l_B^2\right) + B_4 s_3^2\right]\ddot{q}_1 - B_4 c_3 s_3 \ddot{q}_2 \\ &+2B_4 c_3 s_3 \dot{q}_1 \dot{q}_3 + B_4\left(s_3^2 - c_3^2\right)\dot{q}_2\dot{q}_3 \\ &-B_4 c_3 \dot{q}_3 \Omega = -F_y L - k q_1 - f\dot{q}_1 \end{aligned} \quad (1)$$

$$\begin{aligned}\mathcal{L}_{q_2} : &-B_4 c_3 s_3 \ddot{q}_1 + \left(J_2 + m_4 l_A^2 + B_4 c_3^2\right)\ddot{q}_2 \\ &+B_4\left(s_3^2 - c_3^2\right)\dot{q}_1\dot{q}_3 - 2B_4 c_3 s_3 \dot{q}_2 \dot{q}_3 \\ &-B_4 s_3 \dot{q}_3 \Omega = F_x L - k q_2 - f\dot{q}_2 \end{aligned} \quad (2)$$

$$\mathcal{L}_{q_3} : B_4\left(c_3\dot{q}_1 + s_3\dot{q}_2\right)\Omega = T_{23} \quad (3)$$

$$\mathcal{L}_{q_4} : -B_4\left(s_3\ddot{q}_1 - c_3\ddot{q}_2 + c_3\dot{q}_1\dot{q}_3 + s_3\dot{q}_2\dot{q}_3\right) = T_{34} \quad (4)$$

By construction, some of the inertial effects of the gyroscope are negligible compared with some other terms in equations (1) to (4). For instance, the terms $B_4 s_3^2 \ddot{q}_1$, $-B_4 c_3 s_3 \ddot{q}_2$, $2B_4 c_3 s_3 \dot{q}_1 \dot{q}_3$ and $B_4\left(s_3^2 - c_3^2\right)\dot{q}_2\dot{q}_3$ appear to be negligible in equation (1). Analogously, the governing equations of the system can be simplified as following:

$$\begin{aligned}\mathcal{L}_{q_1} : &\left[J_2 + m_4\left(l_A^2 + l_B^2\right)\right]\ddot{q}_1 + f\dot{q}_1 + k q_1 \\ &= c_3 T_G - F_y L \end{aligned} \quad (5)$$

$$\mathcal{L}_{q_2} : \left(J_2 + m_4 l_A^2\right)\ddot{q}_2 + f\dot{q}_2 + k q_2 = s_3 T_G + F_x L \quad (6)$$

with $T_G = B_4 \dot{q}_3 \Omega$.

The gyroscopic torque T_G is proportional to the gimbal speed, the gyroscope speed and its moment of inertia. So it is possible to control the gimbal speed so that it induces the appropriate torque required to compensate for heart motion in real time.

3. SYSTEM DESIGN

3.1 Device description

In the designed compensation system, the passive stabilizer is modeled as a 10 mm-diameter and 300 mm-long steel rod which corresponds to commercial instruments in terms of size and rigidity.

In order to identify the forces that the stabilization system should compensate for, *in vivo* experiments were conducted by Bachta et al. (2008) on an anesthetized swine. Measurements of the forces exerted at the distal-end of a passive stabilizer by the beating heart are reported in Fig. 3. These data reveal that the force and displacement

are prominent along the $\boldsymbol{y_0}$ direction. So we propose to compensate for cardiac effect on the stabilizer along this direction. Note that the forces compensated for using gyroscopic effect vary in the range $0 - 3.5$ N. Concerning frequencies they are mainly composed of a constant value which corresponds to the initial constraint, heart beating frequency (about 1.5 Hz) and its harmonics and breathing frequency (about 0.25 Hz) and its harmonics.

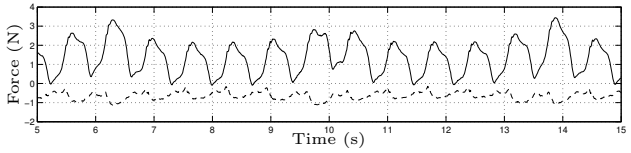

Fig. 3. Heart action along $\boldsymbol{x_0}$ (dashed) and $\boldsymbol{y_0}$ (plain).

Since we want to design a compact and light device with a high gyroscopic effect and considering the equation of the gyroscopic torque, we chose to maximize the gyroscope spin rate in order to avoid the use of a high inertia and powerful motors. In addition the gimbal speed should not be too high in order to keep the system close to its reference position and thus avoid a deviation of the gyroscopic torque. Another important constraint on the design is to provide a motion compensation device compatible with existing passive stabilizer. A CAD view of the designed system complying with the foregoing requirements is presented in Fig. 4.

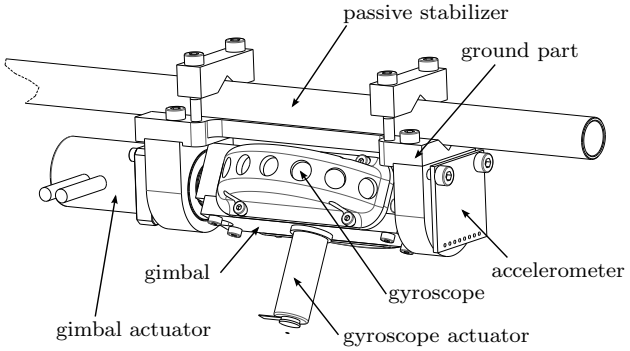

Fig. 4. System CAD overview.

Most of system parts are made of aluminum to improve the lightness except the gyroscope which is made of steel to increase its inertia. The gyroscope is guided on the gimbal thanks to two bearings. The gimbal is composed of two parts and permits to attach the gyroscope motor and protection casings. It is guided on the system ground part by the gimbal motor on one side and a bearing on the other side. This ground part permits also to attach the accelerometer on it and the whole system on the stabilizer.

Static finite element analysis was carried out to validate the proposed design. Each component was successfully analyzed using a worst case scenario. The modal analysis of the whole assembly was also used to confirm the absence of resonant frequencies within the range of operating conditions.

Concerning the control of the gyroscopic device, various sensing solutions are possibly usable: force, position, speed or acceleration sensors, camera. However we chose to use an accelerometer because such a sensor can be easily embedded on the system. Moreover, since its reference is inertial, it does not need any external component linked to the ground as a reference unlike camera, position and speed measurements. It does not require either stabilizer modifications to allow force sensing. And finally, the acceleration measurement is directly linked to the force we wish to compensate for.

Finally the designed system is 130 mm long and wheights 390 g including actuators and sensor. Thus the compactness is clearly improved compared to previous solutions and the device is easily integrable in surgical environment, without inconvenience for the surgeon.

3.2 Influence of system location

The model described in section 2 is a pseudo-rigid-body model which provides a simplified method of analyzing the actual deflection of the stabilizer as explained in Howell (2001). The springs and dampers located at the joints q_1 and q_2 are chosen to have an equivalent force-deflection behaviour. In this case, the gyroscopic torque T_0 needed to compensate for cardiac force is independent from the gyroscope position along the stabilizer and $T_0 = -F_y L$.

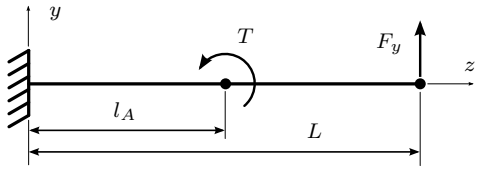

(a) Case I: torque applied on one point.

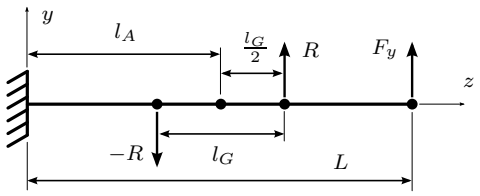

(b) Case II: torque applied on two points (taking account of the gyroscopic system length).

Fig. 5. Continuous beam deformation models.

However, to better account for the actual deflection, we can model the passive stabilizer as a cantilever beam loaded with the force F_y at the distal end point and the torque T_0 applied at a distance l_A from the fixed end as depicted in Fig. 5(a). If the gyroscope length is l_G, the gyroscopic torque T_0 is no longer applied at one point. The resulting model is presented in Fig. 5(b). The deflection and slope of the beam along $\boldsymbol{z}$ are calculated from the linear elastic deformations expressions:

$$\begin{cases} d\theta = \dfrac{M}{EI} dx \\ dy = \theta dx \end{cases}$$

$$\begin{cases} \theta(z) = \dfrac{1}{EI} \displaystyle\int_0^z M(u) du \\ y(z) = \dfrac{1}{EI} \displaystyle\iint_0^z M(u) du \end{cases}$$

where $M(z)$ is the bending moment applied to the section, $\theta(z)$ the beam slope, $y(z)$ the transverse displacement, E

the Young's modulus and I the second moment of area with respect to $\boldsymbol{x}$. To obtain the displacement compensation at the distal point, the acting torque T_0 should be set to verify the condition $y(L) = 0$. The resulting expressions of T_0 for both cases I and II may be written as:

$$T_{0_{\mathrm{I}}} = -\frac{2L^3}{3\,(2L - l_A)\,l_A} F_y$$

$$T_{0_{\mathrm{II}}} = -\frac{2L^3}{3\,(2L - l_A)\,l_A - l_G^2} F_y$$

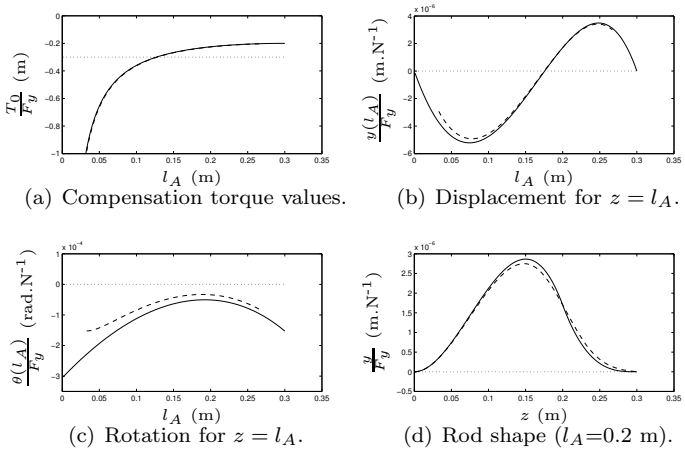

(a) Compensation torque values. (b) Displacement for $z = l_A$.

(c) Rotation for $z = l_A$. (d) Rod shape (l_A=0.2 m).

Fig. 6. Comparison of pseudo rigid model (dotted line), case I (plain line) and case II (dashed) when compensation torque T_0 is applied; l_G=66 mm. Dimensions are compared to F_y

These linear elastic deflection models also provide useful information on the rod deformed shape, the displacement of point A where the gyroscope has been fixed, the rotation of the gyroscope about the axis $(A, \boldsymbol{x})$ and the required torque.

One can notice on Fig. 6(a) that the compensation torques of continuous models decrease when l_A increases, and become smaller than the one from pseudo rigid model for $l_A > 0.13$ m. So it is advantageous to position the system the closest to the distal end.

Since the gyroscopic device is the heaviest part of the system, its displacement and rotation, even if they are small, may induce dynamic excitation of the structure and consequently vibrations. So they should be minimized. From the curves in Fig. 6(b) and 6(c) we can define the minimal displacement for $l_A = 0.18$ m and the minimal rotation for $l_A = 0.19$ m.

Thus minimizing the torque is incompatible with minimizing the movement so a compromise between the both have to be reached. Based on the previous results, positioning the system in the range $l_A = [0.15\ ;\ 0.2]$ m is acceptable. Since the system displacement and rotation are very small we chose to favor a greater torque and we used in the sequel l_A=0.2 m. The corresponding rod deformed shape is depicted in Fig. 6(d).

In addition, since the results for cases I and II are similar, we can assess the system length l_G has no significant influence over the previous dimensions.

4. CONTROL DESIGN AND SIMULATIONS

4.1 Control Issue

The aim is to control the gimbal in order to stabilize the beam position y using the acceleration $\ddot{y}$ given by the accelerometer attached to the system. As can be seen in (5), the torque provided by the gyroscope is proportional to $\dot{q}_3$ and c_3 since Ω and B_4 are constant. So it can be controlled using the gimbal speed as an input. Since the gimbal position is available, we consider in the sequel that the nonlinear c_3 term is compensated for by dividing the control signal before applying it as a reference to $\dot{q}_3$. Therefore, the dynamic equation relative to the parameter q_1 along the $\boldsymbol{y}$ axis may be written as: $J\ddot{q}_1 + f\dot{q}_1 + kq_1 = -k_u\dot{q}_3 - LF_y$ with $k_u = -B_4\,\Omega$ and $J = J_2 + m_4\left(l_A^2 + l_B^2\right)$. For simplicity, let $d = LF_y$ be the perturbing torque exerted by the heart. The global control structure is those depicted in Fig. 7 where the transfer function $H(s)$ is given by:

$$H\,(s) = \frac{k_0 s^2}{s^2 + as + b}$$

with $k_0 = \frac{-L}{J}$, $a = \frac{f}{J}$ and $b = \frac{k}{J}$.

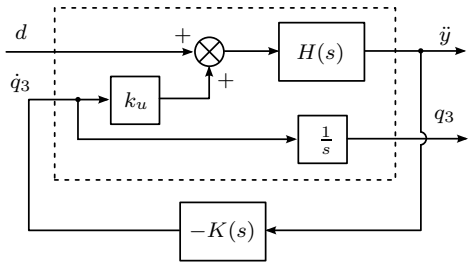

Fig. 7. System structure with dynamic feedback.

The main goal of the control strategy is to reject the effects of the heart beat on the stabilizer movement, i.e. to have the gain of the transfer T_{yd} from heart excitation to position as low as possible within a given bandwidth corresponding to the heart beating frequencies (from 1 Hz to 10 Hz).

The second goal is to keep the position q_3 of the gimbal into interval $[-q_{3_{\max}}\ ;\ q_{3_{\max}}]$. Indeed, the gyroscopic torque direction depends from the gimbal angle and would induce for $|q_3| > \frac{\pi}{4}$ a lower effect on the desired direction than the disturbance on the other direction, i.e. $\boldsymbol{y}$ and $\boldsymbol{x}$ respectively. This problem can be solved by insuring that the transfer $T_{q_3 d}$ from perturbation to gimbal position is finite in low frequency or even low-cut thus avoiding an angle drift.

Notice that the two aims are conflicting as the perturbation rejection requires the use of the control input. Therefore, it is necessary to meet a trade-off between perturbation rejection in the high frequency and free movement in the low frequency.

4.2 Static State Feedback versus Dynamic Output Feedback

In this part speed $\dot{y}$ and position y are obtained from the acceleration measurement $\ddot{y}$ given by the accelerometer. On an experimental system this measurement would be subject to noise and filtered integration or Kalman filtering

would be necessary to obtain speed and position estimation without any drift. For simulation purpose we assume in the sequel the estimations of $\dot{y}$ and y are available.

Let us first consider a static state feedback (SSF) $\dot{q}_3 = -k_1 y - k_2 \dot{y}$. This control law can be seen as a dynamic output feedback (DOF) law $\dot{q}_3(s) = -K(s)\,\dot{y}(s)$ where $K(s) = \frac{k_2 s + k_1}{s^2}$. With this controller, the transfer function from perturbation to gimbal position is given by:

$$T_{q_3 d}(s) = \frac{-k_0\,(k_2 s + k_1)}{s^3 + p_1 s^2 + p_2 s} \tag{7}$$

with $p_1 = k_u k_0 k_2 + a$ and $p_2 = k_u k_0 k_1 + b$. This transfer has infinite gain in the low frequencies and cannot be used because it would imply a drift of the gimbal angle q_3.

This issue can be solved by including in the control a term depending on q_3, leading to the control:

$$\dot{q}_3 = -k_1 y - k_2 \dot{y} - k_3 q_3 \tag{8}$$

Neglecting the initial condition on q_3, one can write $q_3 = \frac{\dot{q}_3}{s}$. Therefore the DOF is $K(s) = \frac{k_2 s + k_1}{s(s + k_3)}$ and the transfer function from perturbation to gimbal angle becomes:

$$T_{q_3 d}(s) = \frac{-k_0\,(k_2 s + k_1)}{s^3 + p_3 s^2 + p_4 s + k_3 b} \tag{9}$$

with $p_3 = k_u k_0 k_2 + k_3 + a$ and $p_4 = k_u k_0 k_1 + k_3 a + b$. Here the gain in low frequency is finite.

A low-pass rejection behavior can be implemented by including the integral of the position :

$$\dot{q}_3 = -k_1 y - k_2 \dot{y} - k_3 q_3 - k_4 I_{q_3} \tag{10}$$

where $I_{q_3} = \int_0^t q_3(\tau) d\tau$. This structure allows zero mean for q_3 in periodic mode even if d has a continuous component.

Notice that the two shapes (SSF and DOF) of the controller are not completely equivalent even if they have the same transfer functions. Indeed, the second form is insensitive to the initial value of q_3 and cannot force q_3 to remain close to zero. Therefore, the first form, i.e. the SSF, must be implemented.

More generally speaking, if a DOF controller is determined under the following form:

$$K(s) = \frac{b_m s^m + ... + b_0}{s^n + a_{n-1} s^{n-1} + ... + a_0} \tag{11}$$

it must be implemented as a SSF including the integrals of the measurements:

$$u = -a_{n-1} I^0_{q_3} - ... - a_0 I^{n-1}_{q_3} + b_m I^{n-m}_{\ddot{y}} + ... + b_o I^n_{\ddot{y}} \tag{12}$$

where $I^k_{q_3}$ denotes the k^{th} integral of q_3.

4.3 Tunning of Linear Quadratic Regulator

We proposed a state representation of the system based on equation (5) and which can be written in the following way:

$$\dot{X} = \begin{bmatrix} 0 & 1 & 0 & 0 & 0 \\ \frac{-k}{J} & \frac{-f}{J} & 0 & 0 & \frac{k_u}{J} \\ 0 & 0 & 0 & 0 & 1 \\ 0 & 0 & 1 & 0 & 0 \end{bmatrix} \begin{bmatrix} X \\ U \end{bmatrix}$$

with $X = [\, y \;\; \dot{y} \;\; q_3 \;\; I_{q_3} \,]^T$ the state vector and $U = \dot{q}_3$.

We used for SSF determination a linear quadratic regulator (LQR) synthesis which minimizes the following cost function:

$$\int_0^\infty \left(X^T Q X + U^T R U\right) dt$$

where R is set as the identity matrix and weightings are set as $Q = \text{diag}([w_1\ w_2\ w_3\ w_4])$. Thus penalties can be set for each state independently. The given solution is a state feedback $U = -KX$ where $K = -R^{-1} B^T P$ with P the solution of the Ricatti equation:

$$PA + A^T P - PBR^{-1} B^T P + Q = 0$$

In order to compute an optimal set of weightings $w_i = 10^{e_i}$, we used a stochastic genetic-like algorithm based on gaussian adaptation. The goal is to minimize the RMS amplitude of y for frequencies higher than 0.5 Hz as performance criterion and to respect the constraint $|q_3(t)| < 45°$. Let write $\boldsymbol{e}^j(k) = [e_1^j(k) \cdots e_n^j(k)]$ where $e_i^j(k)$ is the i^{th} feature of the j^{th} individual $\boldsymbol{e}^j(k)$ of the k^{th} generation and n the number of weightings.

(1) For initialization a population of p individuals $\boldsymbol{e}^j(0)$ is generated randomly.
(2) Simulation is processed for each individual $\boldsymbol{e}^j(k)$. Based on the obtained results the individuals which do not respect the constraint are eliminated and the ones presenting a better performance criterion than the mean are selected.
(3) The mean value $\boldsymbol{m}(k)$ and standard deviation $\boldsymbol{\sigma}(k)$ of the selected subpopulation are computed and a new generation $(k+1)$ of p individuals is generated randomly following the normal distribution $\mathcal{N}(\boldsymbol{m}(k), \boldsymbol{\sigma}(k)^2)$.
(4) The steps (2) and (3) are performed iteratively until $\boldsymbol{\sigma}(k)$ is considered to be small compared to $\boldsymbol{m}(k)$, which guarantees the convergence.

4.4 Simulation and results

The proposed control method was implemented in simulation using the gyroscopic system model with dimensions corresponding to the mechanical design described before. The gimbal actuator dynamics and torque limits are included and the gyroscope speed was set to $50,000$ rpm which fits actuator specifications. The states weighting were tuned using the iterative algorithm described before with $p = 50$ and is close to an optimum: $Q = \text{diag}\left(\left[5.84 \cdot 10^9; 6; 5.6 \cdot 10^{-5}; 18.2\right]\right)$. The results of simulations performed with these parameters are reported in Fig. 8.

To limit transient effects which produce a temporary large gimbal drift the regulation is gradually activated with a slope from 2 to 7 s.

Fig. 8(a) shows a comparison of the y displacement with and without regulation. One can notice that the displacement amplitude is effectively reduced for frequencies higher than 1 Hz. This is confirmed by the frequency decomposition diagram (Fig. 8(b)). The RMS amplitude for these frequencies is divided by 4. The speed results in Fig. 8(c) shows a high damping and the RMS amplitude of $\dot{y}$ is divided by 7.

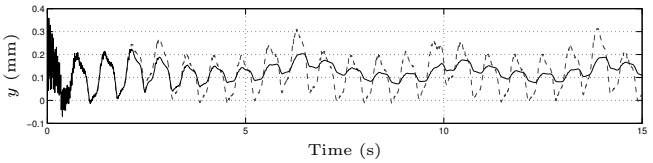

(a) Displacement y of the stabilizer tip.

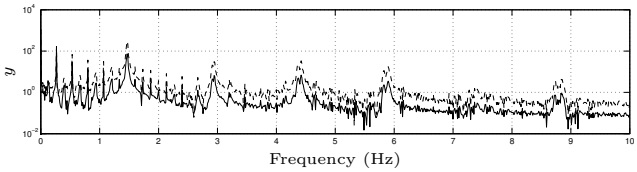

(b) Frequential decomposition of y.

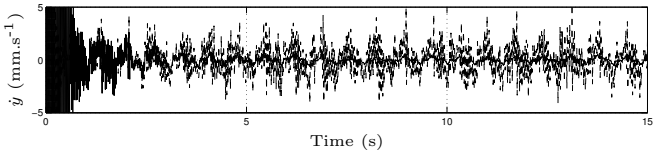

(c) Speed $\dot{y}$ of the stabilizer tip.

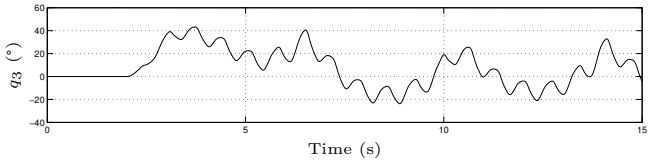

(d) Angular position of the gimbal q_3.

Fig. 8. Tip displacement, displacement frequential decomposition and gimbal angular position. In plain lines with the gyroscopic compensation and in dashed lines without.

The gimbal angle remains into reasonable boundaries ($\max(|q_3|) = 44°$) as shown in Fig. 8(d). Consequently the gyroscope torque does not affect significantly the x position which amplitude remains unchanged.

The fundamental harmonic of the heart beating ($f = 1.5$ Hz) is less damped than the highest ones (for 2.9, 4.4, 5.9, 7.4 and 8.8 Hz). This is due to the trade-off mentioned in § 4.1: the low frequencies cannot be rejected as q_3 must remain in a restricted interval. With the current device, it appears that the cardiac harmonics of rank higher than two can be properly attenuated, but the respiratory components and the fundamental of the cardiac component are not reduced sufficiently. However, solutions are available for the rejection of the low frequencies as in Bachta et al. (2008). Based on proximal actuation, these latter solutions suffer from low bandwidth but are sufficient for the rejection of the respiratory component and of the fundamental of the cardiac component. Therefore, the gyroscopic actuation device could be combined with a more conventional device in order to extend the bandwidth.

5. CONCLUSION

The original concept of a gyroscopic compensation is a good solution to overcome the problem of cardiac motion within the framework of minimally invasive beating heart surgery. The proposed design is fully adaptable and does not need any modification of the surgical instrument. The reduced size (130 mm long) and wheight (390 g) make it easy to manipulate and integrate in surgical environment. The gyroscopic actuation and acceleration sensing, since they are based on inertial effects, make the system independant from any grounded element. In addition the concept can be easily extended to other fields needing similar structure stabilization. The principle and equations was presented, the device design process was described and a first prototype is currently being constructed. A control strategy based on acceleration sensing and using a state feedback calculated thanks to LQR synthesis and taking into account gyroscopic actuation specificities, was simulated. This preliminary study confirmed the feasibility of such a device and its ability to reduce cardiac motion. The prototype should be operative soon and it will be possible to perform experiments in real conditions to validate the concept.

ACKNOWLEDGEMENTS

This work was carried out in the LSIIT laboratory which is a component of UdS and CNRS. It was also possible thanks to the Alsace Regional Council.

REFERENCES

Bachta, W., Renaud, P., Laroche, E., Forgione, A., and Gangloff, J. (2008). Cardiolock: an active cardiac stabilizer, first in vivo experiments using a new robotized device. *Computer Aided Surgery*, 13(5), 243–254.

Higashimata, H., Yamada, M., Kazao, Y., and Namiki, M. (1998). Characteristics of active vibration control system using gyro-stabilizer. *Engineering Structures*, 20, 176–183.

Howell, L. (2001). *Compliant mechanisms*. John Wiley & Sons.

Lappas, V.J., Steyn, W.H., and Underwood, C.I. (2002). Attitude control for small satellites using control moment gyros. *Acta Astronautica*, 51, 101–111.

Lemma, M., Mangini, A., Redaelli, A., and Acocella, F. (2005). Do cardiac stabilizers really stabilize? experimental quantitative analysis of mechanical stabilization. *Interactive CardioVascular and Thoracic Surgery*, 4, 222–226.

Loisance, D.Y., Nakashima, K., and Kirsch, M. (2005). Computer-assisted coronary surgery: lessons from an initial experience. *Interactive CardioVascular and Thoracic Surgery*, 4, 398–401.

Mack, M.J. (2006). Minimally invasive cardiac surgery. *Surgical Endoscopy*, 20, 488–492.

Thornton, B., Ura, T., Nose, Y., and Turnock, S. (2007). Zero-g class underwater robots: Unrestricted attitude control using control moment gyros. *IEEE Journal of Oceanic Engineering*, 32, 565–583.

Townsend, N.C., Murphy, A.J., and Shenoi, R.A. (2007). A new active gyrostabiliser system for ride control of marine vehicles. *Ocean Engineering*, 34, 1607–1617.

Tsai, L.W. (1999). *Robot Analysis: The Mechanics of Serial and Parallel Manipulators*. John Wiley and Sons.

Yano, H., Yoshie, M., and Iwata, H. (2003). Development of a non-grounded haptic interface using the gyro effect. In *Proceedings of the11th Symposium on Haptic Interfaces for Virtual Environment and Teleoperator Systems (HAPTICS03)*.